Technical Paper 3684

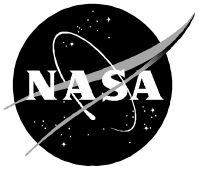

Understanding Skill in EVA Mass Handling

Volume II: Empirical Investigation

P. Vernon McDonald, Gary E. Riccio, Brian T. Peters, Charles S. Layne, and
Jacob J. Bloomberg

July 1997

Technical Paper 3684

Understanding Skill in EVA Mass Handling

Volume II: Empirical Investigation

P. Vernon McDonald and Gary E. Riccio
Nascent Technologies

Brian T. Peters and Charles S. Layne
KRUG Life Sciences

Jacob J. Bloomberg
NASA JSC Life Sciences Research Laboratories

July 1997

National Aeronautic
and Space Administration

Lyndon B. Johnson Space Center
Houston, Texas 77058-4406

Acknowledgments

The investigation described in this report would not have been possible without the expert assistance of several groups and individuals from NASA's Johnson Space Center. We thank the Anthropometry & Biomechanics Facility for providing hardware and technical support for data collection on the precision air bearing floor (PABF). We also wish to thank Tom Smith, Frank Eades, Bill Lee, and John Harvey for their assistance in design and construction of the test hardware, and providing engineering and technical support in all phases of PABF operations. We thank Steve Anderson of ILC Dover for accommodating our investigation into the busy suit schedule, and providing the extravehicular mobility units (EMUs) and EMU technicians during our data collection runs. Special thanks go to our volunteer test subjects who provided their time, expertise, and invaluable comments on our test protocol. We would also like to acknowledge all of those individuals from the extravehicular activity (EVA) operational community with whom we have discussed this project over the course of its progress. We are especially grateful to Jerry Ross, Leroy Chiao, and Jeff Hoffman for permitting an EVA-experienced crew member to participate in our study. This project was support by NASA grant 199-16-11-48.

This publication is available from the Center for AeroSpace Information, 800 Elkridge Landing Road, Linthicum Heights, MD 21090-2934 (301) 621-0390.

Contents

Contents

(continued)

Contents

(completed)

Tables Page

Figures Page

Acronyms

CCD	charge-couple device
COP	center of pressure
DOF	degree of freedom
EMU	extravehicular mobility unit
EVA	extravehicular activity
HUT	hard upper torso
JSC	Johnson Space Center
ISS	International Space Station
LTA	lower torso assembly
ODR	ORU docking receptacle
ODS	ORU docking structure
ORU	orbital replacement unit
PABF	precision air bearing floor
PFR	portable foot restraint
PLSS	primary life support subsystem
WETF	Weightless Environment Training Facility
YAC	yaw axis cradle

Preface

This series of four reports will describe the activities performed in the completion of work funded under the NASA Research Announcement 93-OLMSA-07. The funded project, entitled "Environmental Constraints on Postural and Manual Control" was a 3-year project designed to promote a better understanding of the whole-body skill of extravehicular activity (EVA) mass handling. Summary details of task progress can be found in The Life Sciences Division of the NASA Office of Life and Microgravity Sciences "Life Sciences Program Tasks and Bibliography." The Task Book is available via the Internet at: http://peer1.idi.usra.edu.

The first report in the series, "Understanding Skill in EVA Mass Handling. Volume I: Theoretical & Operational Foundations," describes the identification of state-of-the-art EVA operational procedures and the development of a systematic and uniquely appropriate scientific foundation for the study of human adaptability and skill in extravehicular mass handling.

The second report in the series, "Understanding Skill in EVA Mass Handling. Volume II: Empirical Investigation" describes the implementation and design of an unique experimental protocol involving the use of NASA's principal mass handling simulator, the precision air bearing floor. A description of the independent variables, dependent variables, methods of analysis, and formal hypotheses is provided.

Volume III in the series presents the data and results of the empirical investigation described in Volume II. The final report in the series, Volume IV, provides a summary of the work performed with a particular emphasis on the operational implications of the phenomena observed in our empirical investigation.

Abstract

In this report we describe the details of our empirical protocol for investigating skill in extravehicular mass handling using NASA's principal mass handling simulator, the precision air bearing floor. Contents of this report include a description of the necessary modifications to the mass handling simulator; choice of task, and the description of an operationally relevant protocol. Our independent variables are presented in the context of the specific operational issues they were designed to simulate. The explanation of our dependent variables focuses on the specific data processing procedures used to transform data from common laboratory instruments into measures that are relevant to a special class of nested control systems (discussed in Volume I): manual interactions between an individual and the substantial environment. The data reduction is explained in the context of the theoretical foundation described in Volume I. Finally, as a preface to the presentation of the empirical data in Volume III of this report series, a set of detailed hypotheses is presented.

1. Development of Empirical Design

1.1 Defining an Operationally Relevant Protocol

The primary criterion of the empirical effort pursued within the project *Environmental Constraints On Postural and Manual Control* was to attain maximum operational relevance to the skill of extravehicular activity (EVA) mass handling. To this end, the project investigators engaged in interactions with representatives from the EVA operations community at NASA's Johnson Space Center (JSC) and NASA Headquarters. These interactions were crucial in providing this investigation with a thorough grounding in the lessons learned as a result of NASA's EVA operations to date. Comments from EVA crew members, engineers who design and build EVA tools, EVA trainers, and support staff of the many training facilities at JSC were supplemented with reviews of existing documentation of EVA operational procedures, and EVA mission debriefs. Together, this information was pivotal in shaping the approach we ultimately pursued in this investigation with respect to:

a) the relation between the experiments and operational considerations in EVA
b) the key scientific principles behind the relation between crew member (postural) restraints and mass handling
c) methods that should be used to study the relation between postural restraints and mass handling
d) the design and use of ground-based simulators for the development of EVA skills such as mass handling

1.2 The Mass Handling Simulator

Since this project was a ground-based investigation, it was necessary to simulate the characteristics of mass handling in weightlessness. NASA's primary mass handling simulator is JSC's precision air bearing floor (PABF), which comprises a high-precision stainless steel surface 24 feet wide x 32 feet long made up of 32 steel plates (36x96x6 inches each) leveled to ±.01 inches over the extent of the floor. Masses are supported on sleds equipped with pads, usually placed in a triangular array, through which is forced compressed air. The air forced through the pads raises the sled, and the mass thereon, approximately .003 inches above the floor so that it rides on a cushion of air. Consequently, the mass is moveable with minimal friction in 3 degrees of freedom (DOFs). An additional air bearing, which can be placed onto a sled, is able to add 2 further "frictionless" DOFs, giving a total of 5 DOFs. This air bearing is usually used to support masses which are being handled so that one may better experience the orbital dynamics of mass handling.

1.3 Choice of Task

A central requirement of our task was that it should capture some fundamental elements of EVA mass handling. It was not necessary for the task to look like any actual on-orbit EVA, rather the task should comprise generic components common to any, or most, EVA mass handling. Of course, the task also had to be implemented on the PABF and thus was constrained by the nature of the simulator. We defined a task which entailed the translation of a mass from one body-relative location to another in order that the mass be docked into a docking receptacle. The presence of both translation and docking components in this task meant that it was compatible with many of the on-orbit mass handling activities likely to be confronted. To explore the demands on postural control and manual control, a number of experimental manipulations were necessary. The following sections describe these in detail.

1.4 Enhancement of the Mass Handling Simulator

A pivotal development of the investigation was a modification to NASA's primary mass handling simulator—the PABF. Typically, the PABF has been used for mass handling activities while the "handler" stood upright, or with the handler lying on their side on an air-bearing sled. Each of these configurations pose different postural challenges; however, we considered neither one to be sufficiently comparable to the on-orbit challenges to postural control. In particular, we determined that a crucial aspect of on-orbit postural control entailed managing the postural mobility/stability tradeoff concurrently in orthogonal rotational axes. Since we wished to investigate the role of postural stability, it was crucial that we provide sufficient DOF for

postural movement. The *"yaw-axis cradle (YAC)"* was designed for use with the extravehicular mobility unit (EMU) in the recumbent orientation on the PABF. This provided the necessary additional DOF of postural movement such that subjects were forced to manage the postural mobility/stability tradeoff concurrently in orthogonal rotational axes (i.e., pitch and yaw).

Figure 1 shows a photograph of the YAC frame, and Figure 2 shows the YAC fully integrated into the experimental setup. Figure 3 illustrates a schematic of how the EMU, YAC, and the air-bearing sled were assembled on the PABF. Using body-relative definition of axes of motion, pitch rotation was made available with the air bearing sled in the plane of the PABF, and yaw rotation was available via the mechanical bearings on each end of the YAC. While in the recumbent (left-hand-down) orientation in the YAC, the subject was restrained using a portable foot restraint (PFR) similar to those used on orbit.

The YAC frame was designed such that the axis of rotation would pass through the center of mass of the human-EMU-frame system, and be perpendicular to the axis of the EMU waist bearing (rather than parallel to the longitudinal axis of the hard upper torso unit of the EMU).

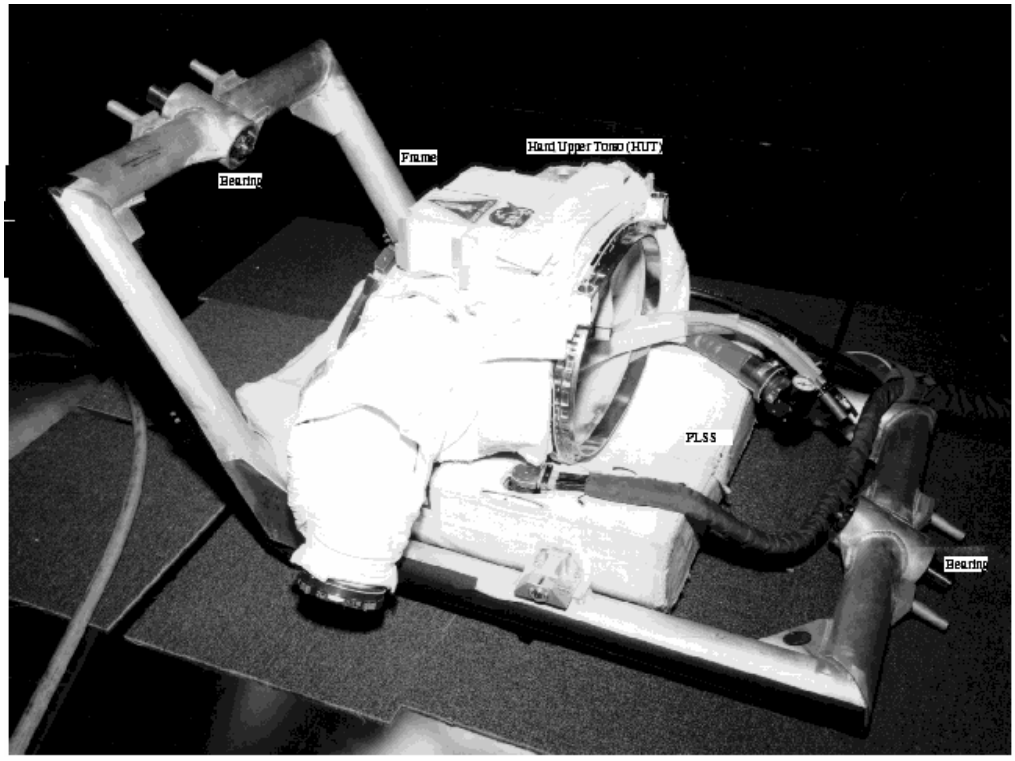

Figure 1. The Yaw axis cradle shown with the HUT element of the EMU inserted. The system is designed such that the axes for yaw rotation run through the center of mass of the subject in the EMU.

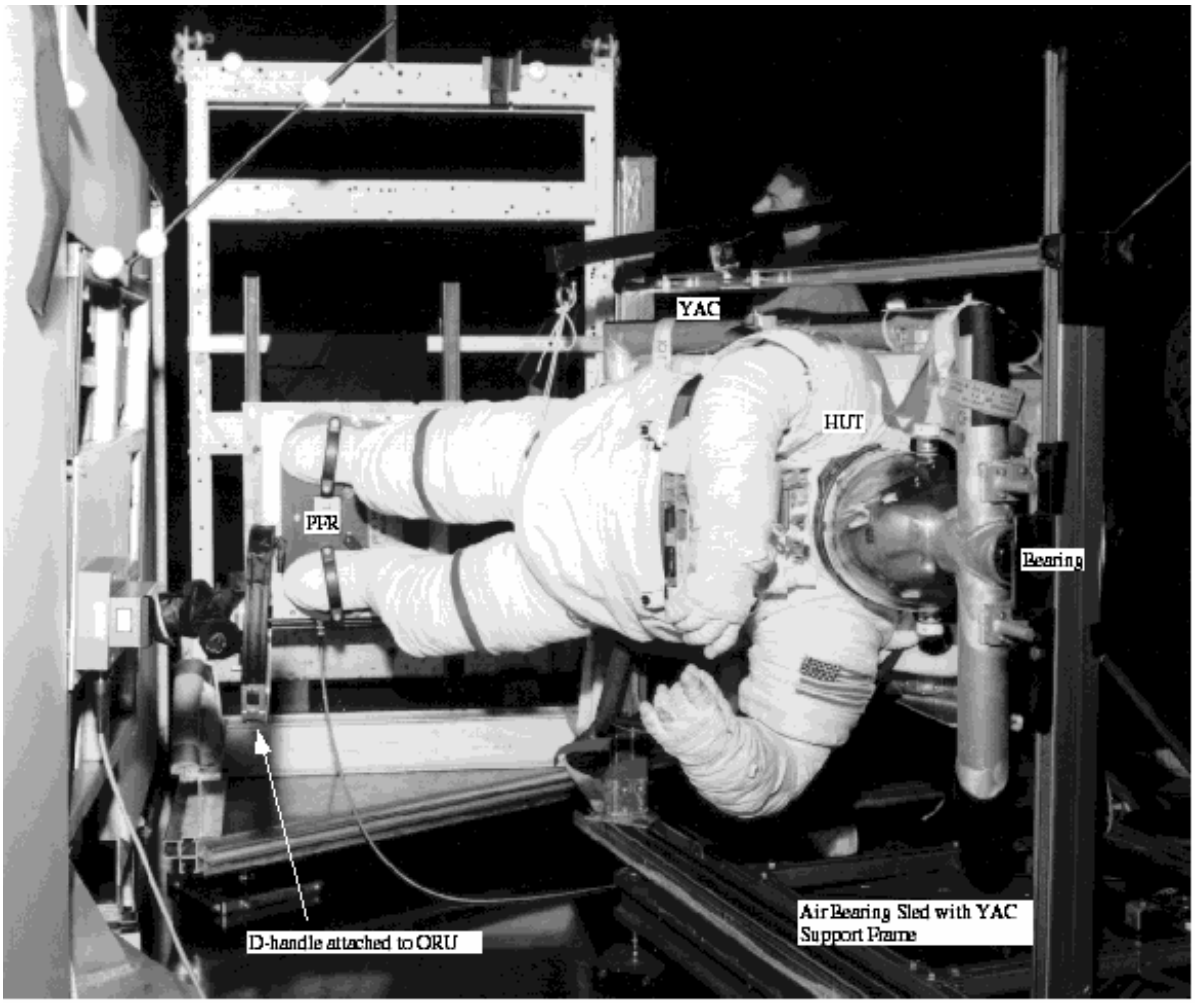

Figure 2. Yaw axis cradle shown in use on the PABF. Subject in EMU in the YAC has just completed a docking trial with the ORU, which is fully inserted into the docking structure.

The aim of this design was to minimize the mass of the counterweight required to attain neutral stability in the yaw axis. One modification that was necessary concerned the tendency for rotation of the lower torso assembly (LTA) toward the floor. This rotation was possible about the EMU waist bearing, which we wished to permit. However, to eliminate the asymmetry, it was necessary to counterweight the LTA. The best method was to support the LTA with a sling connected to a counterbalancing weight cantilevered on the immobile components of the YAC.

As a safety measure, the bearings were limited to ±15 degree rotation by the use of physical stops. However, this limit rarely impaired yaw rotation during subsequent testing to the extent that yaw rotation was within this ±15 degree envelope. Subjects with little or no prior experience in the EMU and in simulated EVA mass handling did not typically notice the yaw motion that they produced during mass handling. However, one subject with prior experience

in these conditions did notice yaw mobility and commented favorably about this attribute of the YAC.

Overall, the YAC appears to be a valuable addition to the complement of devices that are used in the PABF. In particular, it appears to be a valuable enhancement to the simulation of mass handling tasks. Its value is that it provides more of the mobility that is available in EVA. It allows the multiaxis postural perturbations and, thus, the need to stabilize posture that we believe is important to the whole-body skill of mass handling. It should be noted that the YAC reduces the fidelity of EMU inertia in the sagittal plane because additional mass is required to stabilize, against tipping moments, the air-bearing sled that supports the YAC.

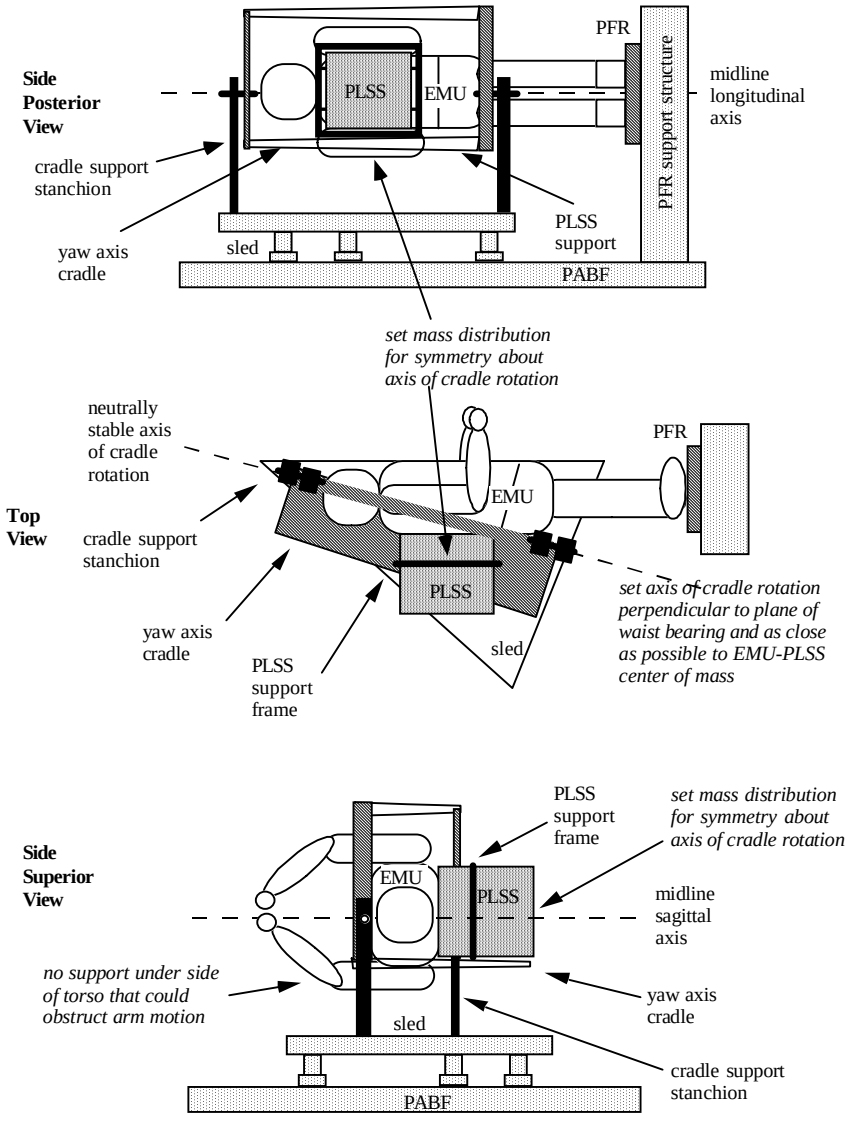

Figure 3. Schematic of YAC-EMU-sled assembly.

2. Experimental Configuration

The components of our experimental configuration comprised a 5-DOF orbital replacement unit (ORU), the YAC-EMU-sled assembly, the ORU docking structure (ODS), and the PFR and its attachment structure. Each component is described below.

2.1 ORU design

The ORU for this test was based upon a generic International Space Station (ISS) component—the Rocketdyne "battery box". This component was to be used in the STS-80 EVAs for evaluation of mass handling tools. The mockup of this ORU was constructed using unistrut and approximated the flight component volumetrically. The mass and inertial properties varied from the flight component. The degree of dissimilarity depended upon the axis of motion. The unistrut frame was supported at the geometric center by an air-bearing ball which permitted limited rotation in pitch, yaw, and roll. The air-bearing ball was in turn supported by an air-bearing sled so that the ORU-sled mass could be translated within the plane of the PABF. The unistrut frame was neutrally balanced by the addition of lead plates within the frame. The entire mass of the ORU was required to be greater than 180 Kg and less than 320 Kg.

A prototype D-handle microconical ORU handling tool was located on the (subject relative) left-superior quadrant of the ORU. Consequently, the midpoint of the handle (i.e., microconical fitting) was *not* located on a principle plane of inertia, such that cross-coupled moments would be encountered upon attempts to move the ORU. The handle was fitted to a 6-DOF force-torque transducer which, in turn, was rigidly attached to the ORU structure. The transducer allowed the measurement of the forces and torques applied to the handle and thus to the ORU during the docking task.

Figure 4 shows the ORU and handle sitting at the opening to the docking structure. The air-bearing ball is hidden by the plate at the center of the ORU. One notable difference of this mockup is its transparency. Typically, crew members cannot see through the ORU they are handling. This of course is a significant constraint on the ability to perform accurate docking tasks. Often in such situations, a second crew member will be positioned for better visibility to guide the crew member handling the ORU.

The ORU was approximately 93 cm square and 41.5 cm deep, and was adjustable to two different heights above the plane of the PABF. One height placed the center of the D-handle such that it was 109.2 cm above the floor and matched the height of the yaw rotation axis of the YAC. Figure 5A illustrates this relationship. The other height placed the center of the D-handle such that it was 99 cm above the floor and matched the height to the center of the PFR.

These two conditions were referred to as the midsagittal condition and the oblique condition respectively. In the midsagittal condition the ORU handle was in a plane coincident with the midsagittal plane of the body. In the oblique condition the ORU handle was in a plane 10 cm closer to the floor (toward the subject's left hand) and parallel to the floor. For comfort, the PFR was offset from the midsagittal axis of the HUT. This is a common practice on the PABF.

2.2 ORU docking structure

A rigid and immobile ODS for the battery-box mockup was constructed from unistrut and assembled such that yielding to the forces encountered during contact with the ORU was minimized. The ODS included a rigid backstop at a depth that was equal to the depth of the ORU. Corners and catch points on the ODR and ORU were eliminated so that docking was as smooth and as operationally valid as possible. The docking structure is seen as the background to the ORU in Figure 4.

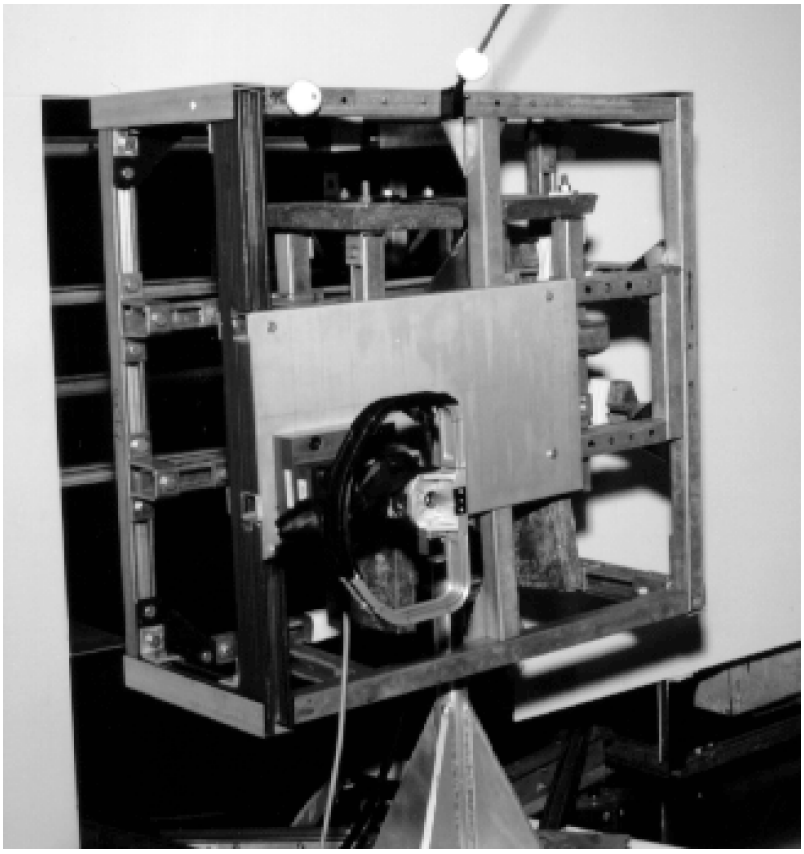

Figure 4. ORU mockup derived from the Rocketdyne battery box.

The ODS was assembled so that the location and size of the ORU docking receptacle (ODR) could be changed. The change in size of the ODR provides docking tasks with variable

amounts of tolerance or difficulty. The change in location of the ODR provided docking trajectories that were either coincident with the midsagittal plane of the EMU, or 10 cm to the left of this plane. The discrete locations of the ODR were set to have specific relationships to the EMU in the YAC (e.g., midsagittal ORU trajectory). Two sizes of the ODR were used to simulate "high" and "low" accuracy docking requirements. In the **high-accuracy** condition, the ODR was 2.5 cm longer and 2.5 cm wider than the ORU. Thus there was a 1.25 cm gap around the ORU when docked optimally in the ODR in the high-accuracy condition. In the **low-accuracy** condition, the ODR was 10 cm longer and 10 cm wider than the ORU. Thus there was a 5.0 cm gap around the ORU when docked optimally in the ODR in the low-accuracy condition. In all conditions, the ODR was framed, for visual purposes, using foam-core sheets. The ODR was structurally framed at the corners with aluminum angle running the entire depth.

2.3 YAC-Sled Assembly

Details of the YAC are described in Section 1.4. The frame of the YAC attached to the primary life support subsystem (PLSS) mockup which, in turn, rigidly attached to the hard upper torso (HUT) unit of the EMU and, thus, essentially became an extension of the HUT. The frame was suspended by the mechanical bearings on each end such that the yaw rotation axis was at a height of 109 cm above the floor. A schematic illustrating the relation of these components is presented in Figure 3. The YAC-EMU system sat upon an air-bearing sled such that the subject in the EMU protruded slightly over the leading edge of the sled. This minimized the interference of the YAC sled with the ORU sled during the docking task. The EMU, and thus the subject, was always placed into the YAC in a left-hand-down orientation. Once in the YAC, the subject's feet were locked into the PFR, and the LTA counterbalancing was performed. Figure 5B shows this setup in relation to the ODS and the ORU. The YAC assembly permitted 4 potential DOFs of postural movement. However, in some trials, we eliminated DOFs by locking out the potential for yaw rotation and/or by turning off the air for the sled. Consequently, without yaw rotation there were only 3 potential DOFs of postural movement. With the additional absence of the air-bearing sled, there were essentially 0 potential DOFs of postural movement. This latter condition required the mass handling task to be completed using hands and arms only.

2.4 PFR and Attachment Structure

While in the recumbent orientation in the YAC, the subject was restrained using a PFR similar to those used on orbit. The feet were restrained during all phases of this investigation. The

PFR was attached to a superstructure with a mass in excess of 1000 Kg. This superstructure also possessed sufficient rigidity so that there was no noticeable yielding to forces and torques applied through the PFR. The PFR attachment structure was set on an air-bearing sled to permit relocation of the PFR to one of six positions which were used to vary the location of the feet relative to the ODS. The PFR was instrumented with a 6-DOF force-torque transducer. The transducer allowed the measurement of the forces and torques applied to the PFR during the docking task. During testing, the PFR was positioned in one of six locations relative to the ODS. These six locations were referenced to the height and reach of each subject so as to place the performer in more or less optimal regions of a work envelope defined on the basis of their reach geometry. Figure 5C illustrates the relative configurations of each of the components described in the previous sections.

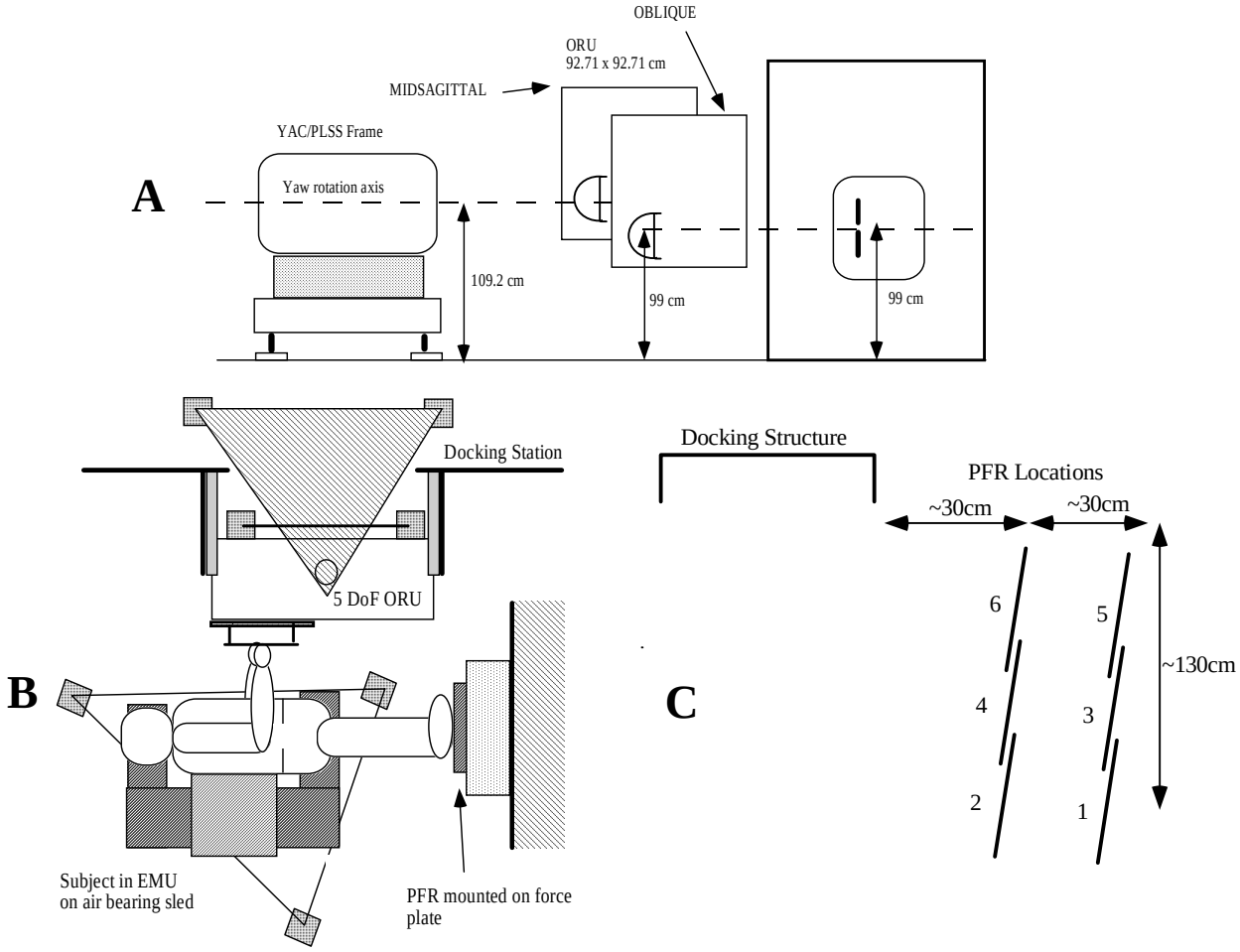

Figure 5. Schematic showing the layout for the PABF test of mass handling.

3. Experimental Manipulations

The following section describes the independent variables of the PABF investigation of EVA mass handling skill. Each independent variable was designed to simulate a specific operational issue. The relation between the independent variables and the operational issues is summarized in Table 1.

Table 1. Operational Issues Evaluated By Way of Experimental Manipulations

Operational Issue	Experimental Manipulation
Limited worksite access	6 discrete PFR locations
Worksite layout & access	2 ORU trajectories
Task constraints	Docking accuracy
Choice of restraint system	0, 4 postural DOF
Simulator fidelity	3, 4 postural DOF
Crew member skill	Subject mix

3.1 PFR location

The PFR location was varied through 6 different locations. Figure 5C illustrates the relative position of each location. The intent of this manipulation was to vary the location of the feet relative to the ODS. This has the associated effect of varying the postural configuration necessary for performing the docking task. This manipulation was designed to simulate the operational constraint of restricted worksite access. For any orbital EVA there are finite PFR locations available in the Shuttle payload bay (the same will be true for ISS). While a PFR attached to the RMS permits substantially more flexibility, the RMS is not always available. Consequently, crew members will commonly be forced to work from a PFR placement which results in manual tasks being performed in a nonoptimal region of the manual workspace. When the RMS is available, it would be useful to have guidelines for the accuracy of PFR placement.

3.2 ORU Trajectory

The ORU trajectory was varied by changing the height of the ORU relative to the PABF surface. In subject relative terms there were two trajectories, one coincident with the midsagittal plane of the body (midsagittal condition), and the other shifted 10 cm toward the left hand (toward the floor) so that the ORU would move the plane to the left of and, upon yaw

rotation, not necessarily parallel to the midsagittal plane. Again, worksite clutter and layout may demand nonoptimal trajectories of ORUs which are being transported from one location to another. This manipulation was designed to evaluate the consequences of such trajectories. Figure 5A illustrates the planes of motion of the ORU relative to the PFR and the plane of the PABF.

3.3 Docking Accuracy

Docking accuracy was set at two different tolerances. The high-accuracy condition entailed docking the ORU with a 1.25 cm clearance on all sides. The low-accuracy condition entailed docking the ORU with a 5.0 cm clearance on all sides. The operational counterpart of this manipulation can be seen in the various tasks crew members have to complete under various task constraints. For example, some of the Hubble Space Telescope repair activities demanded highly accurate transport in light of the delicate instrumentation within the telescope and within the ORU. Other mass handling scenarios may be less demanding on manual precision.

3.4 Postural Degrees of Freedom

Three conditions were possible: 4, 3, and 0 DOFs. The combination of the YAC and the air-bearing sled permitted motion in 4 postural DOFs: body pitch and yaw, and anterior-posterior and superior-inferior translation. No roll or medio-lateral translation was possible. With the yaw rotation eliminated (using physical restraints), only 3 postural DOFs were available: body pitch, and anterior-posterior and superior-inferior translation. By turning the air off, the air-bearing sled became fixed in place, and 0 postural DOFs were available. In this case the docking task had to be completed with arm motion only.

Operationally these postural DOF manipulations are equivalent to activities in which a crew member has a number of restraint options available. NASA is currently developing a semirigid tether that attaches to the miniworkstation on the HUT of the EMU. This device can be used alone to provide a small degree of restraint, or it could be used in conjunction with the PFR to essentially provided restraints at two locations: feet and torso. The latter scenario could eliminate the majority of body motion—similar to our 0-DOF manipulation. The use of the PFR restraint on orbit is most closely resembled by our 4-DOF manipulation in which there is the possibility of cross-coupled perturbations in orthogonal axes of motion. The 3-DOF manipulation is an important comparison condition for the purpose of validating the fidelity and utility of the YAC.

3.5 Subject Skill Level

Subjects were all volunteers, who had passed the Air Force Class III physical and had undergone the NASA Physiological Training program. Subjects were primarily selected to cover a broad range of EVA-related, suited, mass handling experience. Of the five subjects selected, two were complete novices to the extent that their only experience of EVA mass handling occurred within the context of this investigation, and was thus limited to activities on the PABF. One subject had previously performed suited mass handling on the PABF. One other subject had previously performed suited mass handling on the PABF, in the Weightless Environment Training Facility (WETF), and on the KC-135 aircraft during parabolic flight. Consequently these two subjects had some experience of EMU activities in all the available simulators. The fifth subject had the most extensive range of experience, having performed on-orbit EVAs. This subject had performed four Shuttle mission EVAs for a total of 25 hours of on-orbit EVA.

4. Procedures and Data Collection

The following describes the procedures, transducers, and data sources used in the PABF investigation of EVA mass handling skill. A matrix of the trial sequence is also provided.

4.1 EMU fitting

The EMU used for PABF testing was a CLASS III EMU, virtually identical to the CLASS I system used on orbit. Differences between the two included the absence of operating monitoring systems in the CLASS III and a PLSS mockup, since air and cooling were provided by remote means. Prior to EMU operations, anthropometric measurements were made so that an appropriately sized EMU could be constructed. The EMU comprises multiple components, each of which can vary in size, according to the proportions of the wearer. Note that the gloves are the one item which are personally sized and manufactured for each EVA crew member. For our purposes, the non-crew member subjects were issued “off-the-shelf” gloves.

After the EMU was assembled, each subject proceeded through a “fit” check to validate the fit and comfort of the EMU. While the EMU can be adjusted for different individuals, there are still important differences with respect to mobility within the EMU. Fit and mobility of particular body segments within the EMU also are influenced by postural configuration (and by postural orientation in a terrestrial environment). Arm extension, for example, influences the extent to which hands are “pushed into” the gloves and, thus, it influences prehensile capabilities. For our purposes, this simply meant that arm extension was a stronger constraint

on postural configuration than without an EMU. In other words, subjects may adapt postural configuration to a greater degree so that they can maintain or achieve an arm orientation that optimizes prehensile ability. This emphasizes further the limited relevance of factors affecting maximal strength for our investigation. The postural dependence of segmental fits in the EMU probably will create an asymmetry when subjects are lying on their sides in the EMU. Our prediction is that for equal fit of left and right hand-in-glove, the "lower" arm will have to be extended more than the "upper" arm. To the extent that this is the case, the difference in difficulty between the oblique docking trajectory (i.e., ORU lower than the subject above the floor) and sagittal docking trajectory may be less than between the equivalent trajectories in weightlessness.

A representative from ILC Dover—the contractor responsible for fitting the EMU to different crew members—indicated there are significant individual differences in mobility inside the EMU even though there are quite a few adjustments that can be made to fit the EMU to each individual, and that it is not unusual for anthropometric dimensions to influence the selection of crew members for particular EVA mass handling tasks. The implication of this is that the postural constraints on mass handling performance will differ among crew members. At the same time, the consequences of mass handling for postural stability will differ among crew members because of individual differences in the fit of the EMU.

For the novice subjects, the fit check was their first experience of ingressing the EMU, and of being pressurized inside the EMU. The pressure used was 4.3 psi, identical to the current on-orbit EMU operating pressure. This made the suit "stiffness" comparable, although the history of use can also affect this stiffness. The fit check provided an opportunity for the novice subjects to "move" about under the constraints of the EMU joints. Notably these suit joints do not map directly onto the joints of the human body. Consequently, one aspect of skilled behavior in the EMU is learning how to work "with" the EMU so as to exploit the joint geometry, rather than fight against it.

4.2 Kinematics

Kinematic data were collected using both videography and accelerometry. Details of both procedures are described below.

4.2.1 Videography

Kinematic data were collected with a video-based motion analysis system. The technique for three dimensional video motion analysis uses the two-dimensional images from multiple

cameras and the known orientations of those cameras relative to each other to reconstruct the three-dimensional location of desired points. For our investigation, we used the HiRes system manufactured by Motion Analysis Corporation, Santa Rosa, California. This system utilizes the visible light spectrum to illuminate retro-reflective spheres. These spheres are attached to those items whose motion one wishes to track. The HiRes system is highly automated and has the ability to track the motion of multiple retroreflective spheres, or markers, placed within the field.

Five NEC TI-23A black-and-white charge-couple device (CCD) cameras captured our video images. The cameras were evenly spaced, radially along a 110^{O} arc around the center of the work space. The distance of the cameras from the arc's center was dependent on the camera's lens. In an effort to place the cameras in areas where there would be minimal chance of them being in the way or being accidentally moved, a combination of 4.8, 8, and 12 mm lenses were used. Each camera/lens combination was precalibrated to map any nonlinearities and/or any lens distortions. These were corrected algorithmically before calculating the movement trajectories. The cameras were also equipped with electronic shutters that stopped the motion to .001 seconds. To eliminate any temporal discrepancies in the video data collection, the shutter opening for all of the cameras was synchronized at 30 Hz. The video data were collected for 25 to 35 seconds per trial, according to the proficiency of the subject, and the individual two-dimensional video images were processed in real time. This process resulted in a digital file from each camera containing a two-dimensional location of each marker in the CCD plane at a sample rate of 30Hz. Post-processing of these files is described below.

There are three main steps in the three-dimensional reconstruction process: calibration, tracking, and editing. All of these steps are a part of the software of the HiRes system. The calibration step, identified here, differs from the camera/lens calibration mentioned earlier. This calibration is the process of identifying the position and orientation relationship between the cameras. We accomplished this by collecting video data of a cube with eight markers, whose locations were measured to within 0.0002 mm, before each data collection session. By identifying a minimum of 6 of these markers from each camera view, the software calculates the camera locations, in a coordinate system defined by the cube, and saves the information to be used in the processing of subsequent files. The tracking step combines the individual camera files of two-dimensional marker information and the camera calibration information so as to determine the three-dimensional location of each marker in each frame of data. Spurious reflections in the field of view and markers whose view is obstructed during portions of the trial can produce inconsistencies in the data output of the tracking process. These issues are addressed using the graphical interface of the editing process.

The completion of calibration, tracking, and editing results in a file containing the X, Y, and Z trajectories (as defined by the calibration cube) of each of the reflective markers. The accuracy of the HiRes system has been verified in our lab to be better than 1 in 2000 under ideal conditions. For our experimental setup, with a field of view of approximately 4 meters, the measurement accuracy is estimated in the order of 2 mm.

The requirements defined in our experimental design required the relative motions of four objects be monitored: the ORU, PFR, ODS, and YAC. By tracking the motion of three non-collinear markers per object, whose relationship to each other was fixed, we were able to capture the motion in 6 DOFs: X, Y, and Z as well as roll, pitch, and yaw. Using fewer than three markers reduces the number of DOF of the motion that can be determined. The markers themselves were attached to each object with either double-sided tape or secured to rods which were affixed to the object. Maximizing the distance between the markers served to improve the system's ability to resolve rotational movements.

4.2.2 Accelerometery

In order to monitor YAC rotation, two ±5 g Entran EGA3-5D triaxial accelerometers were attached to the YAC. One accelerometer was placed on the lower (subjects' left side) side of the frame, the other on the upper side (subjects' right side) of the frame. The accelerometers were located equidistant from the yaw rotation axis. Each accelerometer was amplified by an "in-line" amplifier located within 30 cm of the transducer. The immediate amplification was necessary, given the long cable length to the A/D system. Analog data were sampled via a 12-bit A/D system at a rate of 500 Hz. These data were stored to the hard drive of a portable computer. Before each data collection session, transducer calibration determined the gain and bias for each axis of the two accelerometers. Gains were approximately 1.9 v/g.

4.3 Kinetics

Two AMTI 6-DOF force-torque transducers were used to measure the kinetics at the PFR and at the ORU handle. Interface fittings permitted rigid attachments between the transducers and the other structures. All orientation definitions are body-relative. Data from both transducers were sampled via a 12-bit A/D system at a rate of 500 Hz. These data were stored to the hard drive of a portable computer and temporally synchronized with the accelerometer sampling.

4.3.1 PFR

The PFR transducer was oriented such that positive Fx corresponded to an anterior force; positive Fy was a force to the right; and positive Fz was a force "down" (or inferior).

Amplification was set at maximum such that full-scale deflection in Fz corresponded to ±5800 Newtons, and full-scale deflection in Fx and Fy corresponded to ±2900 Newtons.

4.3.2 ORU

The ORU transducer was oriented such that positive Fx corresponded to a superior force; positive Fy was a force to the right; and positive Fz was an anterior force. Amplification was set at maximum such that full scale deflection in Fz corresponded to ±5800 Newtons, and full scale deflection in Fx and Fy corresponded to ±2900 Newtons.

4.4 Data Synchronization

A critical aspect of the data collection was the synchronization of the kinetic and kinematic data. This synchronization was accomplished by collecting a digital output signal from the video system to an analog data channel. This normally high digital signal was changed to a square-wave during the video data collection. The falling edge of each square wave cycle was coincident with the shutter opening of the cameras, thus providing an analog time stamp for each video sample. Because the analog and video data collection systems were triggered by independent triggers, the analog data was collected for 40 seconds per trial. This longer data collection period was used to provide a time buffer at the beginning and end of each analog data trial to assure that the start and end of the video data collection would always be captured on the analog channel.

4.5 Subjective Ratings

Subjective comparisons among simulator configurations and conditions was an important component of the investigation. Participation of a crew member was important because it provided for comparisons of the mass handling experiment with true weightlessness. Such comparisons were intended to be somewhat open-ended and to be conducted at each subject's convenience. In addition, more constrained assessments were made immediately after particular trials. Separate ratings of ORU and EMU handling qualities, for example, were made after each trial. During PABF mass handling, subjects participated in conditions with 0, 3, and 4 postural DOFs. There were consecutive trials in these configurations at each ORU position. This permitted direct comparisons among the configurations after each set of trials. To facilitate this formal rating and the acquisition of informal ad hoc comments, the communications link with the subject in the EMU was recorded using the audio input of the videotape recorder which simultaneously recorded a surveillance view of the experiment from a camera with an overhead view of the PABF.

4.6 Trial Sequence

Table 2 illustrates the number and type of trial performed by each subject. The differences in the number and type of trials performed by certain subjects was a function of contingencies occurring at the time of data collection. In each of the experimental conditions—trajectory, accuracy, and postural DOFs—there were six different positions of the PFR relative to ODS. Zero postural DOFs indicates that the YAC was locked and air was off for the sled. Three DOFs indicates that the YAC was locked and air was on for the sled (this provides a direct evaluation of our PABF innovation). The postural DOFs were always manipulated within each PFR location before changing to another PFR location. Each subject participated in at least two 90- to 120-minute experimental sessions to complete all trials. The two sessions were not always on the same day.

Table 2. Trials Performed in Each Condition by Each Subject

				2 Novice Non-Crew	Expert Non-Crew (PABF)	Expert Non-Crew (PABF,WETF & KC-135)	Expert Crew (On Orbit)
Dock Trajectory	Dock Accuracy	Postural DOF					
sagittal	high	0		1 x 6	1 x 6	1 x 6	2 x 6
sagittal	high	3		1 x 6	1 x 6	1 x 6	1 x 6
sagittal	high	4		3 x 6	2 x 6	1 x 6	3 x 6
sagittal	low	4		3 x 6		2 x 6	
oblique	high	0		1 x 6	1 x 6	1 x 6	2 x 6
oblique	high	3		1 x 6	1 x 6	1 x 6	1 x 6
oblique	high	4		3 x 6	3 x 6	2 x 6	4 x 6
oblique	low	4		3 x 6	3 x 6		
				96 trials per subject	78 trials	54 trials	78 trials

The trial sequence was randomized by trajectory, accuracy, and PFR location. The postural DOF manipulation was consistent to permit comparisons with preceding trials. Thus a typical trial/condition sequence is shown in Table 3.

Table 3. Example Condition-Trial Sequence

Trajectory (random)	Accuracy (random)	PFR Location	Degrees of Freedom Sequence for Each PFR Location	Trial
Sagittal	Low	1 - 6 randomly selected	4 - 4 - 4	1-18
Sagittal	High	1 - 6 randomly selected	0 - 3 - 4 - 4 - 4	19-48
Oblique	High	1 - 6 randomly selected	0 - 3 - 4 - 4 - 4	49-78
Oblique	Low	1 - 6 randomly selected	4 - 4 - 4	78-96

5. Data Processing

This section describes the data analyses applied to the kinematic and kinetic data measures. The theoretical foundation for this analysis strategy is described in Volume I (Section 3.3)[1].

5.1 The Matrix of Variables in the Reduced Data Sets

Table 4 describes the "primary" data sets that are derived from the raw time-histories for the data collected in the mass handling experiments. The assignment of variables into rows and columns is somewhat arbitrary. The row and column codes (A1:G21) are used to facilitate communication about individual cells or groups of cells in the table. The columns in the table can be conceptualized as bundles of variables that take into account the data-collection device (i.e., force plate, accelerometer, video) and the hypothetically important observables (i.e., ORU control, postural configuration, postural stability). Categories of dependent variables are listed in the header of the table (abbreviations are explained in the footnote to the table). Each symbol refers to a category of dependent variable because they summarize activity on more than one axis of motion (e.g., body pitch, body yaw) and because there are a number of ways to summarize such activity (e.g., mean, standard deviation).

[1] Riccio, G.E., McDonald, P.V., Peters, B.T., Layne, C.S., & Bloomberg, J.J. (1997). Understanding Skill in EVA Mass Handling. Volume I: Theoretical & Operational Foundations.

All variables in the reduced data sets are transformations or summaries of the data channels in the raw time-history files. Underlined symbols in the table header indicate variables that are derived through transformation of the data channels at every data point in the raw time-histories. Rows correspond to particular summary statistics that are computed from intervals of data in the raw time-histories. *Each reduced variable is a time-history specified at a 2 Hz update rate*. Each data point in the reduced data sets is determined through computation of a summary statistic over a 0.5-second interval from the corresponding raw time-histories. The number of data points from which these summaries are calculated depend on the sampling rate in the raw time-history (e.g., summaries are based on 250 data points when the sampling rate is 500 Hz). Figure 6 illustrates the steps in this process with an exemplar time series.

Specific dependent variables correspond to particular axes and particular summary statistics which are described in successive rows of the table. Grayed-out cells in the table indicate that there is not a variable for the corresponding combination of axis, summary statistic, and category of variable that is both necessary and sufficient for testing a priori hypotheses. Entries in the cell describe which of the six DOFs of motion are invoked by each particular combination. Relevant DOFs are described in body-relative terms.

Table 4. Matrix of Dependent Variables for the Study of Mass Handling Skill
(see text for details)

		Primary data Sets	ORU Control	ORU control	Postural Config.	Postural Stability	Postural Stability	Postural Stability	Force Couples
			Kinetics	Video	Video	Video	Accel.	Kinetics	Combined
2 Hz Summary	Reference axis		F_O M_O $\underline{\Sigma}_O$	D_O θ_O $\underline{\Sigma}'_O$	θ_U θ_L	$\mathbf{D_U}$	A_1 A_2 $\underline{\mathbf{A}}_U$ $\underline{\boldsymbol{\alpha}}_U$	F_S M_S $\underline{\mathbf{C}}_S$ $\underline{\tau}_S$	$\underline{E}_S$ $\underline{E}_O$ $\underline{\Omega}_{OS}$
		Codes	A	B	C	D	E	F	G
mean	x(t)	1		**corners**	**pitch**				
mean	y(t)	2			yaw				
mean	z(t)	3							
s.d.	dx(t)/dt	4		**corners**				m-l	**pitch**
s.d.	dy(t)/dt	5				s-i	**yaw**		
s.d.	dz(t)/dt	6				**a-p**	**a-p**	**a-p**	**roll**
skew.	dx(t)/dt	7						m-l	**pitch**
skew.	dy(t)/dt	8				s-i	**yaw**		
skew.	dz(t)/dt	9				**a-p**	**a-p**	a-p	**roll**
kurt.	dx(t)/dt	10						m-l	**pitch**
kurt.	dy(t)/dt	11				s-i	yaw		
kurt.	dz(t)/dt	12				a-p	a-p	a-p	roll
corr.	dx(t)/dt	13							
corr.	dy(t)/dt	14					yaw		
corr.	dz(t)/dt	15				a-p	a-p	**a-p**	
lag	dx(t)/dt	16							
lag	dy(t)/dt	17					yaw		
lag	dz(t)/dt	18				a-p	a-p	a-p	
sum	x(t)	19	m-l, pch						pitch
sum	y(t)	20	s-i, yaw						
sum	z(t)	21	a-p, roll						roll

F => measured force, M => measured moment, $\underline{E}$ => equivalent composite force, $\underline{\Omega}$ => noncoplanarity of force couples
$\underline{C}s$ => center of pressure relative to pedal boundaries, $\underline{\tau}$ => time to contact for Cs, {underlines connote derived quantities}
D => linear displacement or position, θ => angular displacement or position, Σ and Σ' => summaries of all measures and axes
A => linear acceleration or tilt relative to gravity, $\underline{\alpha}$ => angular acceleration, {bold indicates necessary and sufficient variables}
O => ORU, S => pedal support surface, U => upper (torso segment or shoulder point), L => lower (legs)
m-l => mediolateral axis re body, s-i => superior-inferior axis re body, a-p => anterior-posterior axis re body
x(t) => time history for above parameters relative to the x-axis in the body-relative coordinate system for that parameter
y(t) => time history for above parameters relative to the y-axis in the body-relative coordinate system for that parameter
z(t) => time history for above parameters relative to the z-axis in the body-relative coordinate system for that parameter
mean => mean of all samples over 0.5 s intervals in raw data, s.d. => standard deviation of all samples over 0.5 s intervals in raw data
skew. => skewness of all samples over 0.5 s intervals in raw data, kurt. => kurtosis of all samples over 0.5 s intervals in raw data
corr. => autocorrelation of all samples over 0.5 s intervals in raw data, lag => time lag for maximal autocorrelation

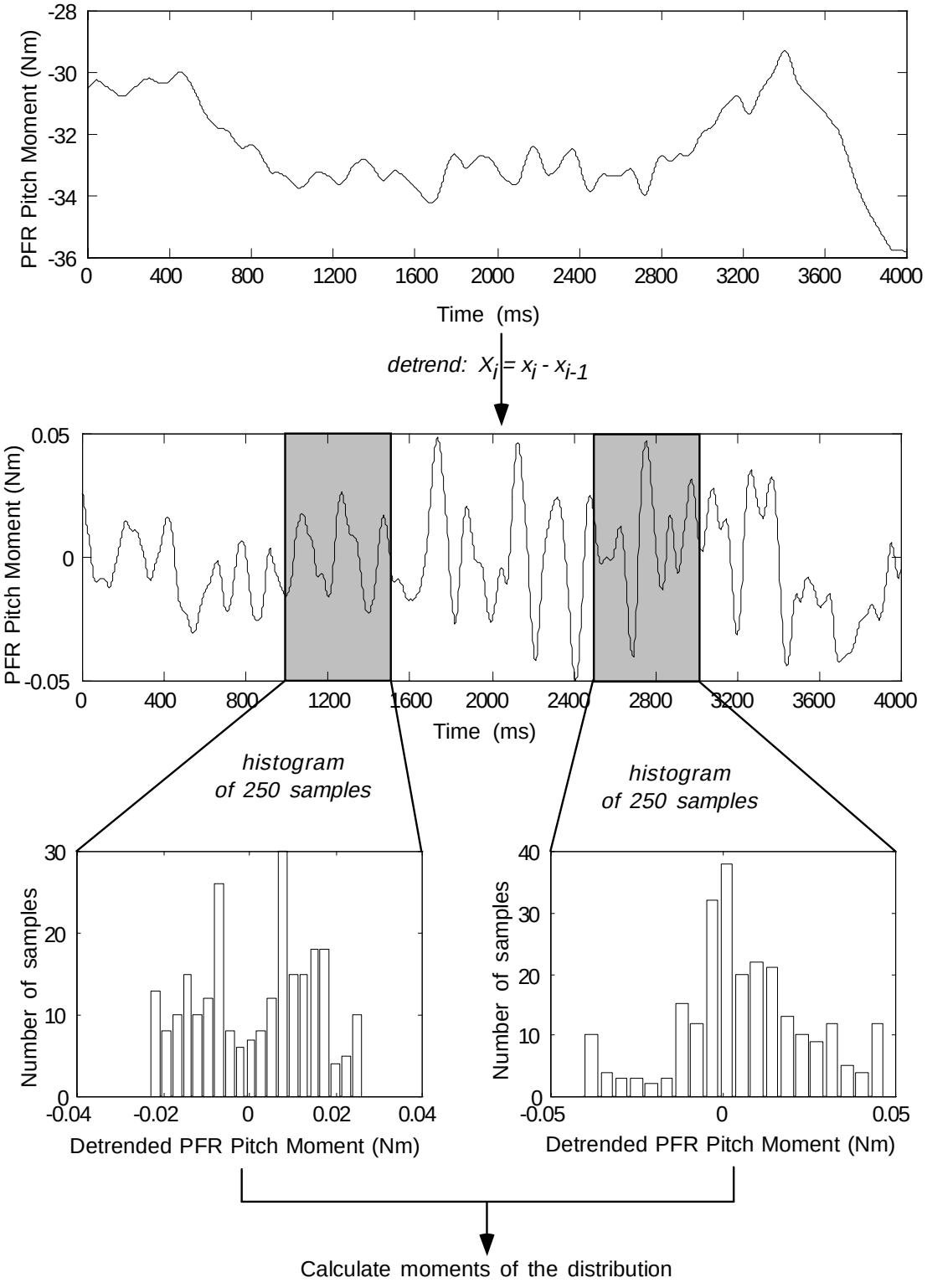

Figure 6. Procedure for deriving update interval distribution moments. Distributions are shown only for two update intervals for clarity. However, distributions are calculated for contiguous update intervals throughout the trial.

5.2 Explanation and Justification for Reduced Variables

Column A (ORU control kinetics): $\underline{\Sigma}_O$ is a summary of the forces and moments measured at the ORU force plate. This summary variable could be useful insofar as it is unnecessary to test ORU-control hypotheses separately on forces and moments. $\underline{\Sigma}_O$ is monotonically related to the energy in ORU translation and docking. Such an energy-related variable is relevant to the softness of the docking and, thus, it is relevant to the task of the subject.

Column B (ORU control kinematics): $\underline{\Sigma}'_O$ is a summary of the linear and angular displacement between the ORU and a fully docked position. This variable is relevant to the smoothness of docking and, thus, it is relevant to the task of the subject. $\underline{\Sigma}'_O$ in cell ranges B1:B3 and B4:B6 each collapse to a single observation per update interval in the reduced data sets.

Column C (postural configuration kinematics): For the purpose of this analysis it was sufficient to consider the human-EMU as a two-segment system (see Riccio & Stoffregen, 1988, and Riccio, 1993, for justification). The upper body was defined as the segment joining the shoulder and hip; the lower body was defined as the segment joining the hip and the ankle. Analyses focus on body configuration in the sagittal plane (i.e., pitch angles of the upper and lower body, θ_U and θ_L). θ_U was defined as that angle between the upper and lower segments. θ_L was defined as that angle between the lower segment and the plane of the PFR.

Columns D & E (postural stability kinematics): D_U is a summary of the body displacement defined as the motion at the EMU "shoulder." It is important to evaluate stability at the shoulder insofar as this region of the body provides the base of support for the head and arms. The accelerations measured on the YAC, A_1 and A_2, were used to derive the degree of yaw rotation occurring, $\underline{\alpha}_U$ during a trial, in particular the degree of yaw stability.

Column F (postural stability kinetics): $\underline{C}_S$ and $\underline{\tau}_S$ are measures derived from the center of pressure on the pedal force plate. $\underline{C}_S$ is the distance of the center of pressure from the nearest pedal boundary. $\underline{\tau}_S$ is the instantaneous time-to-contact between the center of pressure (COP) and the nearest pedal boundary. These variables are potentially valuable as measures of postural stability (see Riccio, 1993, pp. 328-331). Variables from the raw force-plate time-histories need not be retained in the reduced data sets when the boundary-relative measures (e.g., time-to-contact) are used. Analysis of the boundary-relative measures currently is being given a low priority in the mass handling experiments. Instead, we are relying on an expedient measure from the raw data-channels retained in the reduced data sets: the location of the COP relative to the origin of the force plate.

Column G (force couple dynamics): $\underline{E}_S$ and $\underline{E}_O$ are composite force vectors computed from forces and moments at the two force platforms. All moments measured at one force plate are transformed into equivalent forces at the other force plate using an expedient rigid-body assumption. Clearly the human body is not rigid, and the link between the force plates at the ORU and feet is not rigid. If it were, there would be no need to derive composite force vectors because we know that the forces at the two locations would be equal and opposite. We invoke the notion of a rigid body/linkage not as an assumption about our experimental situation but, rather, as a baseline or standard against which nonrigidity, or its correlates, can be measured. One cannot simply compare force-to-force and moment-to-moment between the two locations to assess rigidity or equilibrium. All forces and moments must be reduced to commensurable units to determine, from these data alone, whether the system is in equilibrium.

$\underline{\Omega}_{OS}$ is a measure of the departure from equilibrium of the forces and moments at the hands and feet. We are striving for a method of comparing forces and moments at two locations in (end-points of) a distributed system (the human body) because we assume that the human perceptual systems do this in controlling posture and in coordinating postural control and manual control while interacting with the environment. We assume that a stable postural platform is necessary for effective interactions with the environment (e.g., manual control) and, thus, that the action (including the forces and moments) at the feet and hands must be controlled with respect to the criteria of postural stability. Our strategy of measuring departure from equilibrium in terms of forces and moments at the hands and feet can be viewed as an operational definition of the *observable and meaningful consequences of coupled actions at the hands and feet*. We hypothesize that alignment of the composite vectors in a couple ensures postural stability, as if the body were rigid. Nonalignment or noncollinearity suggests instability, instability that is restricted to a particular plane when the nonaligned vectors are coplanar. We further hypothesize that noncoplanar vectors are especially destabilizing because of their tendency to induce concurrent perturbations in orthogonal axes.

5.3 Explanation and Justification for Task-Relevant Cells in the Matrix

Cells B1:B6 and A19:A21. The purpose of cells A19:A21 was addressed above in the paragraph on $\underline{\Sigma}_O$ and $\underline{\Sigma}'_O$. The purpose of cells B1:B6 is to summarize the smoothness of mass handling. Smoothness of force and motion time-histories is revealed by the spread of data within an interval. Smoothness can be summarized by computing the standard deviation on the detrended data within an interval. These reduced time-histories are being used in assessing the relationship between postural control and manual control. Time-histories for a particular parameter can be reduced to a single parameter per trial by computing summaries (e.g., the mean) of the within-interval standard deviation across all intervals within a trial.

Cells C1:C2. These cells describe changes in postural configuration on a reduced time scale (i.e., 2 Hz). This allows for a point-by-point comparison between postural configuration and various derived indices of postural stability, postural equilibrium, and manual control (described below). The relationships between postural configuration and these indices indicate the way in which these indices are used or can be used as criteria for control of postural configuration (Riccio, 1993, pp. 332-349). Analyses focus on body configuration in the sagittal plane (i.e., pitch angles of the upper and lower body, θ_U and θ_L).

Cells D5-E6. It has been argued that manual control, and even oculomotor control, ultimately must be coordinated with postural control (Riccio, 1993, pp. 343-349; Riccio & Stoffregen, 1988). In particular, it is important to evaluate stability at the shoulder insofar as this region of the body provides the base of support for the head and arms. Stability of posture in the sagittal plane (anterior-posterior and superior-inferior axes) can be assessed in terms of the standard deviation of the detrended position of the shoulder as indicated in the videographic data, D_U. Sagittal stability also can be assessed in terms of the standard deviation of translational acceleration of the YAC as indicated in the accelerometer data, $\underline{A}_U$ (Riccio et al., 1993). Yaw stability can be evaluated in terms of the relationship between the anterior-posterior data from the two accelerometers, $\underline{\alpha}_U$. These parameters are computed over the same intervals as other derived measures and, thus, they are reduced to the same (2 Hz) time scale. This allows for a point-by-point comparison between postural stability and various derived indices of manual control and postural configuration. The relationships between postural stability and manual control indicate the importance of a stable base of support for the arms during mass handling. Analyses focus on postural stability in the anterior-posterior and yaw axes. Particular attention will be given to interactions between these axes, that is, in terms of concurrent motion and instability at these axes. In addition, time-histories for a particular parameter can be reduced to a single parameter per trial by computing summaries (e.g., the mean) of the within-interval standard deviation across all intervals within a trial.

Cells F4 and F6. Postural stability can be considered as the smoothness of relevant force and motion time-histories and, as such, it can be revealed by the spread of data within an interval. Smoothness can be summarized by computing the standard deviation on the detrended data within an interval. Stability of the body as a whole can be assessed in terms of the standard deviation of the detrended center of pressure, $\underline{C}_S$, or related measure, $\underline{\tau}_S$, at the pedal force plate (anterior-posterior and medio-lateral axes). These parameters are computed over the same intervals as other derived measures and, thus, they are reduced to the same (2 Hz) time scale. This allows for a point-by-point comparison between postural stability and various derived indices of manual control and postural configuration. The relationships between postural stability and manual control indicate the importance of stability of the whole body during mass

handling. Analyses focus on postural stability in the anterior-posterior axis. In addition, time-histories for a particular parameter can be reduced to a single parameter per trial by computing summaries (e.g., the mean) of the within-interval standard deviation across all intervals within a trial.

Cells G4 and G6. Stability of the body as a whole can be assessed in terms of the standard deviation of the nonalignment of the pedal-manual force couple, Ω_{OS}, in the roll and pitch axes. These parameters are computed over the same intervals as other derived measures and, thus, they are reduced to the same (2 Hz) time scale. This allows for a point-by-point comparison between postural stability and various derived indices of manual control and postural configuration. The relationships between postural stability and manual control indicate the importance of stability of the whole body during mass handling. Particular attention is being given to interactions between the two axes of noncoplanarity, that is, concurrent change and instability at these axes. The noncoplanar interactions within the force couple are compared with the multiaxis interactions in postural motion mentioned in the preceding paragraph. In addition, time-histories for a particular parameter can be reduced to a single parameter per trial by computing summaries (e.g., the mean) of the within-interval standard deviation across all intervals within a trial.

Cells in block D7:G12. Higher-order statistical moments, skewness and kurtosis, are computed for the same detrended data on which the standard deviation is computed (i.e., cells in block D4:F7). Skewness can be used as a measure of departure from equilibrium, while kurtosis can be used as a measure of intermittency of control (Riccio et al, 1993; Riccio & Stoffregen, 1991, pp. 215-216). These statistics are computed over the same intervals as other derived measures and, thus, they are reduced to the same (2 Hz) time scale. This allows for a point-by-point comparison between the various indices of postural control. The relationships between postural configuration and skewness of postural control, for example, indicate the way in which such indices are used or can be used as criteria for control of postural configuration (Riccio, 1993, pp. 332-342). In addition, time-histories for a particular parameter can be reduced to a single parameter per trial by computing summaries (e.g., the mean) of the within-interval skewness or kurtosis across all intervals within a trial.

Cells in block D14: F18. Enhanced or pathological tremor is assessed in terms of the auto-correlation parameters for the detrended kinematic and kinetic data on postural control. These statistics are computed over the same intervals as other dependent measures and, thus, they will be reduced to the same (2 Hz) time scale. This allows for a point-by-point comparison between tremor and the various indices of postural and manual control. Relationships between tremor and postural configuration, for example, could indicate something about the relative difficulty

or effortfulness of various postural configurations. Analyses will focus on anterior-posterior and yaw axes where available. Time-histories for a particular parameter can be reduced to a single parameter per trial by computing summaries (e.g., the mean) of the within-interval autocorrelation magnitude or lag across all intervals within a trial.

Cells G19 and G21. Noncoplanarity is assessed at the moment of contact between the ORU and ODS. This interval of noncoplanarity is compared to the standard deviation of noncoplanarity over the preceding intervals within trial. The comparison provides an indication of the extent to which the relationship between pedal and manual forces is perceived and the extent to which it is controlled and optimized during docking.

6. Hypotheses

This section formally presents the hypotheses addressed within the context of the empirical investigation described in this report. These hypotheses are implicit within the empirical description in Sections 1-5 and the material presented in Volume 1 of this report series[1].

6.1 Mass Handling Simulators and Manual Performance

These hypotheses are primarily concerned with identification and measurement of manual performance on the PABF. Comparisons of adaptive postural control in the support of manual performance will be made during tasks performed on the PABF with the performer affixed to the PFR:

- There are differences between 3-DOF and 4-DOF simulators with respect to ORU control during the docking phase.
- There are differences between 3-DOF and 4-DOF simulators with respect to postural control during the docking phase.

6.2 Adaptive Postural Control and Manual Performance

These hypotheses are primarily concerned with identification of adaptive postural behavior and measurement of performance on the PABF. Evaluations of adaptive postural control in the support of manual performance will be made during operations on the PABF during which the performer has the opportunity to adaptively configure DOF in response to the task requirements:

- The chosen configuration in the 0-DOF condition is based on the relation between configuration and stability that is revealed in the 3-DOF condition.

- ORU control in the 0-DOF condition is influenced by the relation between configuration and stability that is revealed in the 3-DOF condition.

6.3 Restraint Systems and Manual Performance

These hypotheses are primarily concerned with evaluation of manual performance while the performer is restrained to 0 or 4 postural DOF:

- There are differences between O-DOF and 4-DOF restraint conditions with respect to ORU control during the docking phase.
- There are interactions between restraint DOF and PFR locations with respect to ORU control during the docking phase.

6.4 Adaptive Postural Control During EVA Mass Handling

These hypotheses primarily address the effectiveness and form of adaptive postural control in relation to skill level, ORU handling constraints, and support surface reaction forces:

- There are differences between novice and expert with respect to the interactions between yaw and pitch accelerations.
- There are differences between novice and expert with respect to the kinetics of postural control.
- There are differences between sagittal and oblique ORU trajectories with respect to ORU control and postural control.
- There are differences among PFR locations with respect to ORU control and postural control.
- There are differences between high-accuracy and low-accuracy conditions with respect to ORU control and postural control.

6.5 Interactions Between Postural Control and Manual Control

These hypotheses primarily address the form of adaptive control of the interacting posture and manual systems during the co-variation of manual task criteria and support surface constraints:

- There is a relationship between postural configuration and the kinetics of postural control during the transport phase across PFR locations.
- There is a relationship between postural configuration and the kinematics of postural control during the transport phase across PFR locations.

- There is a relationship between postural configuration and the ORU control during the transport phase across PFR locations.
- There is a multiplicative interaction between yaw and pitch accelerations with respect to ORU control.

6.6 Operational Relevance and External Validity

These hypotheses primarily concern phenomenal/experiential assessments that reveal and enhance the operational relevance and the external validity of this project:

- The experimental task is experientially similar to a variety of tasks performed during EVA.
- There are experiential differences between sagittal and oblique ORU trajectories.
- There are experiential differences among PFR locations.
- There are experiential difference between high-accuracy and low-accuracy conditions.

7. References

Riccio, G. (1993). Information in movement variability about the qualitative dynamics of posture and orientation. In: K. Newell (Ed.), Variability and Motor Control (pp. 317-357), Champaign, IL: Human Kinetics.

Riccio, G., Lee, D., & Martin, E. (1993). Task constraints on postural control. In S.S. Valenti (Ed.), VIIth International Conference on Event Perception and Action (pp. 306-310). Vancouver Canada: Erlbaum.

Riccio, G. & Stoffregen, T. (1988). Affordances as constraints on the control of stance. Human Movement Science, 7, 265-300.

Riccio, G.E., & Stoffregen, T.A. (1991). An ecological theory of motion sickness and postural instability. Ecological Psychology, 3, 195-240.